ELSEVIER

Thermochimica Acta 299 (1997) 67–80

thermochimica acta

Effective work functions of polycrystalline refractory metals heated for thermal positive-ionic and electronic emissions

Hiroyuki Kawano*, Kiyohiko Funato, Seiji Matsui, Keiko Ogasawara, Hajime Kobayashi, Yongfa Zhu[1]

Department of Chemistry, Faculty of Science, Ehime University, Bunkyo, Matsuyama, 790-77, Japan

Abstract

A molecular beam of diatomic metal halide (MX, e.g., LiCl, NaBr, KF, RbBr, CsF, TlCl or InI) was directed onto a polycrystalline surface of refractory metal (e.g., W or Re) heated in high vacua, and the ion current of M^+ emitted from the surface was measured as a function of either (1) surface temperature ($T \approx 800$–2300 K), (2) the elapsed time ($t \approx 0$–10^3 s) after having made the surface essentially clean, or (3) the introduced gas pressure ($P \approx 10^{-5}$–10^{-3} Pa) of air or oxygen, while the sample beam flux (N) incident upon the surface was kept constant in the range of 10^{12}–10^{14} molecules cm^{-2} s^{-1}. The data thus achieved were analyzed by our theory to determine the effective work function (ϕ^+) for ion emission. In addition, the work function (ϕ^e) for electron emission from each surface was measured under various conditions, thereby making it possible to determine the thermionic contrast ($\Delta\phi^* \equiv \phi^+ - \phi^e$). The values of [$\phi_0^+$, ϕ_0^e and $\Delta\phi_0^*$ in kJ mol^{-1}] determined with an essentially clean surface of each metal heated to a high temperature (usually above ca. 1800 K) in a readily attainable high vacuum (2×10^{-5} Pa) are as follows; Nb [463 ± 10, 388 ± 5 and 75 ± 10], Mo [480 ± 6, 424 ± 4 and 56 ± 6], Ta [493 ± 5, 413 ± 5 and 80 ± 5], W [504 ± 5, 434 ± 6 and 70 ± 6], and Re [530 ± 5, 476 ± 5 and 54 ± 5]. With decreasing temperature (usually from ca. 1800 to 1400 K), both ϕ^+ and ϕ^e become higher by up to ca. 100 kJ mol^{-1} than ϕ_0^+ and ϕ_0^e, respectively, mainly owing to the adsorption of residual gases (especially of oxygen). However, $\Delta\phi^*$ itself remained virtually constant at $\Delta\phi_0^*$ with little dependence upon T, t, P and N in the above respective ranges.

Keywords: Polycrystalline refractory metal surfaces; Thermal electron emission; Thermal positive ion emission; Thermionic contrast; Work function

1. Introduction

When a molecular beam of diatomic metal halide (MX) is directed onto a positively-biased surface of polycrystal metal heated to a high temperature (T) in a high vacuum, positive ions (M^+) are emitted after thermal equilibria $MX \rightleftarrows M + X$ and $M \rightleftarrows M^+ + e^-$) have been established on the surface consisting of a large number (i) of patches with different work functions (ϕ_i) and fractional areas (a_i). In this case, the ionization efficiency (β^+) of MX is a steep function of ϕ^+ in stead of ϕ^e. Here, ϕ^+ and ϕ^e are the effective work functions for thermal positive-ionic and electronic emissions, respectively, and they are given [1] by

$$\phi^+ = RT \ln[\Sigma a_i \exp(\phi_i/RT)] \quad (1)$$

$$\phi^e = -RT \ln[\Sigma a_i \exp(-\phi_i/RT)] \quad (2)$$

both of which are different from the simple average

*Corresponding author. Fax: 81-89-927-9590; e-mail: kawano@dpc.ehime-u.ac.jp

[1]On leave from Department of Chemistry, Tsinghua University, Beijing, 100084, P.R. of China.

PII S0040-6031(97)00138-X

work function defined as

$$\overline{\phi} = \Sigma a_i \phi_i \quad (3)$$

It is essentially clean surfaces of a single crystal alone that satisfy $\phi^+ = \phi^e = \overline{\phi}$. It should be noted that the individual values of both ϕ_i and a_i can hardly be determined theoretically or experimentally with any polycrystal surface under a given experimental condition. Generally, ϕ^+ is larger than ϕ^e because M^+ and e^- are emitted predominantly from those patchy faces having higher and lower work functions, respectively [1]. Therefore, theoretical evaluation or estimation of β^+ needs the data on ϕ^+ instead of ϕ^e. It should be emphasized that both ϕ^+ and ϕ^e of any surface are subject to change by adsorption of sample molecules and/or residual gases and hence that they are usually different from those (ϕ_0^+ and ϕ_0^e) of the surface kept essentially clean [1]. Therefore, it is very important to elucidate the subject of how ϕ^+ and ϕ^e depend upon the various conditions employed during experimental studies.

In contrast to the data on ϕ_0^e, however, those on ϕ_0^+ as well as ϕ^+ can hardly be found in thermochemical or thermionic tables published to date. This is mainly because it is very difficult to determine either ϕ_0^+ or ϕ^+ accurately. In order to improve this status, β^+ for a great many sample/surface systems has been measured carefully under various experimental conditions, and the data thus achieved have been analyzed to determine both ϕ_0^+ and ϕ^+ by our theory on thermal positive ionization [2]. Under the same conditions, both ϕ_0^e and ϕ^e have also been determined from the slope of a Richardson plot obtained with each surface.

This paper summarizes the experimental data and analytical results achieved with five refractory metals and also outlines the essential features of the thermionic contrast ($\Delta\phi^* \equiv \phi^+ - \phi^e$) that is very interesting and important in the field of surface science.

2. Experimental

A schematic diagram of our instrument is shown in Fig. 1, where F is a filament (2 cm long) of either Nb, Mo, Ta, W or Re (0.013–0.020 cm in diameter and 0.0032–0.0052 cm^2 in ionizing surface area). A molecular beam of MX effusing from a Knudsen cell kept

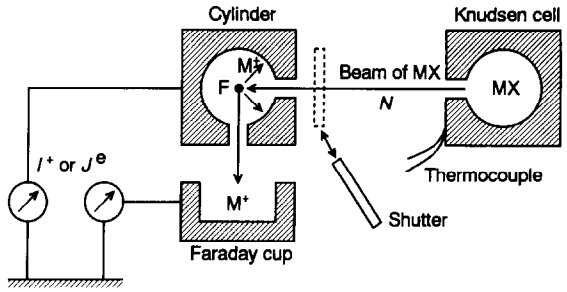

Fig. 1. Schematic diagram of the instrument.

at a constant temperature was directed onto F at a constant flux (N). The ions (M^+) emitted from F were collected mainly with a cylinder and partly (ca. 1%) with a Faraday cup. The cylinder was cooled to ca. 0°C by circulating ice water to suppress the evaporation of MX gradually accumulating inside it. The maximum sensitivities of the electrometers connected to the cylinder and cup were 0.1 nA and 10 fA, respectively. The filament and cell temperatures (T and T_c) were determined with an optical pyrometer and calibrated alumel–chromel thermocouples, respectively. In the final vacuum ($P \approx 2 \times 10^{-5}$ Pa) attained with an oil diffusion pump through a liquid nitrogen trap, the residual gases (RG) mainly consisted of H_2O, CO, O_2, CO_2, and hydrocarbons [3]. The bias potentials applied to F were 50 and −300 V to extract M^+ and electron (e^-), respectively.

To examine the effect of adsorption of RG and/or MX upon F, the ionic or electronic current (I^+ or J^e) was measured as a function of time according to the following procedures. Namely, (1) F was flashed at ca. 2300 K for several minutes with a beam shutter closed in order to remove all adsorbates, (2) the shutter was opened immediately after F was adjusted to a working temperature (T), and (3) without changing any of T, T_c and P, I^+ was measured as a function of the time (t) elapsing after the opening. In a similar way, J^e was measured without sample beam incidence.

In order to check the adsorption effect mentioned above, I^+ or J^e was measured as a function of the pressure (P_a or P_0) of air or oxygen admitted through a needle valve.

According to the above simple methods, both I^+ and J^e were successfully measured as a function of either T, t, P_a or P_0, thereby yielding new data on both ϕ^+ and ϕ^e.

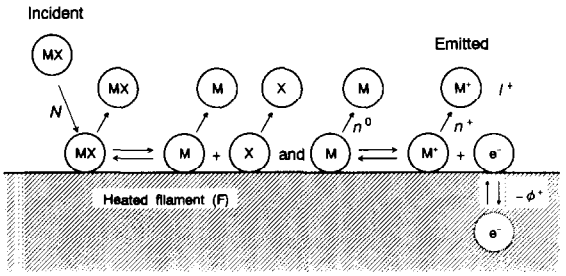

Fig. 2. Illustration of thermal positive ion emission from a heated metal surface.

3. Theoretical

When M^+ is produced from MX incident on a glowing metal surface, as illustrated in Fig. 2, Eqs. (4)–(7) are theoretically derived from our simple model on the ionization [2].

$$I^+ = eSN\beta^+ \tag{4}$$

$$\beta^+ \equiv n^+/N = \sigma\gamma\varepsilon^+ = \sigma\gamma\alpha^+/(1+\alpha^+) \tag{5}$$

$$\alpha^+ \equiv n^+/n^0 = \exp[\Delta S^+/R]\exp[(\phi^+ - I)/\mathrm{RT}] \tag{6}$$

$$\frac{\gamma^2}{1-\gamma} = \frac{1.01\times 10^6 N_A(1+\alpha^+)}{\sigma N(2\pi\mu RT)^{1/2}} \times \exp\left[\frac{\Delta S}{R}\right]\exp\left[\frac{-D}{RT}\right] \tag{7}$$

Here, e is the elementary electric charge; S is the ionizing surface area; N, n^+ and n^0 are the number of MX incident upon F, of M^+ emitted from F, and of M evaporating from F, respectively, per $cm^2\ s^{-1}$; σ is the sticking probability of MX to F, usually taken as unity [1]; γ and ε^+ are the degrees of dissociation of MX and ionization of M, respectively; α^+ is the ionization coefficient of M; ΔS^+ and ΔS are the entropy changes due to ionization of M and dissociation of MX, respectively; I is the ionization energy of M; N_A is Avogadro's number; μ is the reduced weight of MX; and D is the dissociation energy of MX.

Consequently, ϕ^+ can be determined from experimental data (I^+ and T) because thermochemical data (I, D, ΔS, etc.) are readily cited from published tables [4,5] and also the other factors (e, μ, S, etc.) are known to us. It should be noted that the ionization efficiency is usually evaluated from $\beta^+ = I^+/I_m^+$, where I_m^+ is the saturation current independent of T in an optimum temperature range (OTR) [6] so long as T_c is kept constant. In addition, the correspondence of I_m^+ to $\beta^+ = 1$ has has been confirmed by measurements of the vapor pressure of MX in the Knudsen cell kept at T_c [7–9].

Since the thermal electron current (J^e) emitted from F heated to T is given by

$$J^e \propto T^2\exp[-\phi^e/RT] \tag{8}$$

ϕ^e can be determined from the slope of a Richardson plot of $\log J^e/T^2$ vs. $1/T$ [1].

4. Results and discussion

4.1. Temperature dependence

Typical examples observed with the NaCl/W system heated in a high vacuum ($P \approx 2\times 10^{-5}$ Pa) are shown in Fig. 3, where T is successively increased or decreased every ca. 10 min. In OTR ($T_1 - T_2$), I^+ is kept at I_m^+, as already mentioned above. As N increases from 1.6×10^{13} up to 2.2×10^{14} molecules $cm^{-2}\ s^{-1}$, I_m^+ increases from ca. 9 to 120 nA, as shown by curves (1)–(4) in Fig. 3(A). The relation of $\beta^+ = I^+/I_m^+$ yields Fig. 3(B), showing that curves (1)–(4) above $T_2 \approx 1400$ K well overlap with each other and hence β^+ in the range is independent of N. Below ca. 1300 K, on the other hand, the lowest temperature (T_1) keeping $\beta^+ \geq 0.99$ increases with an increase in N and hence β^+ at a given temperature below T_1 becomes smaller as N increases. Generally, I^+ attains an appreciable value around the appearance temperature (T_0) corresponding to $\beta^+ = 0.01$. The threshold temperature range (TTR, $T_0 - T_1$) as well as OTR is usually dependent upon the species of sample/surface system and also upon the experimental conditions employed (see Table 1). To determine ϕ^+ with the system, the data in Fig. 3(B) are theoretically analyzed according to both Eqs. (5)–(7) and thermochemical values (I, D, etc.) cited from tables [4,5], thereby yielding Fig. 3(C). The essential points to be derived from the above data in adding to previous results [10–12] may be summarized as follows:

1. In the high temperature range above T_3 (ca. 1950 K), ϕ^+ is independent of both T and N, and hence, $\phi^+ \approx 500$ kJ mol^{-1} corresponds to the work function (ϕ_0^+) of an essentially clean surface of W.

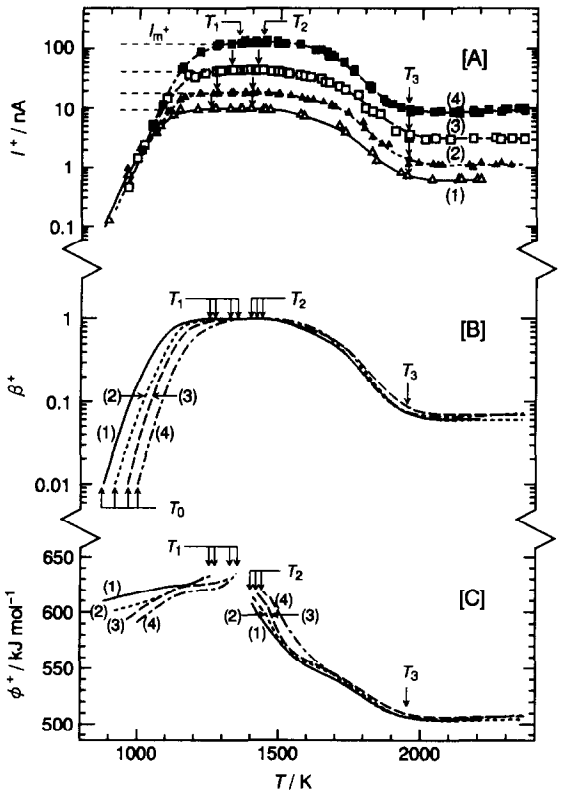

Fig. 3. Surface temperature (T) vs. (A) the ion current (I^+) of Na^+ produced from NaCl incident upon W, (B) the ionization efficiency (β^+) of NaCl, and (C) the effective work function (ϕ^+) of W. Further information about curves (1)–(4) is given in their corresponding rows in Table 1.

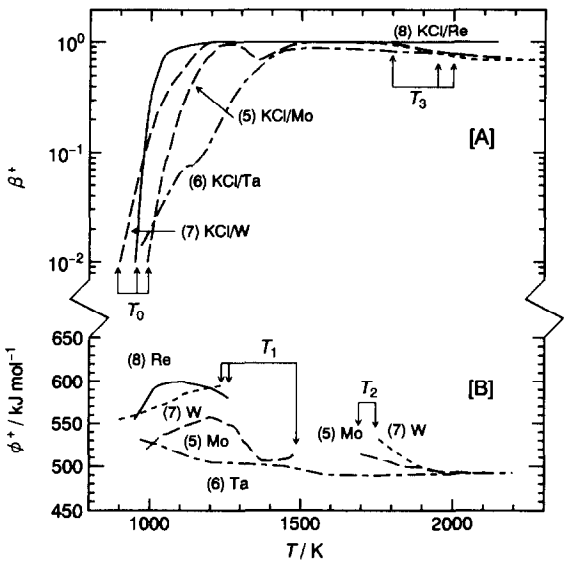

Fig. 4. Temperature dependence of (A) the ionization efficiency (β^+) for the production of K^+ from KCl on four different metal surfaces and (B) the effective work function (ϕ^+) of the surfaces. For further information about each curve, see Table 1.

2. As T decreases from T_3 to $T_2 \approx 1400$ K, ϕ^+ increases by up to ca. 100 kJ mol^{-1} mainly by adsorption of RG.
3. With decreasing temperature from T_1, ϕ^+ decreases by coadsorption of RG and MX. It should be noted that ϕ^+ in OTR cannot be evaluated correctly from Eqs. (4)–(7) because both γ and ε^+ are larger than 0.99.

The boundary temperature $(T_0 - T_2)$ governing TTR $(T_0 - T_1, \beta^+ = 0.01\text{–}0.99)$ and OTR $(T_1\text{–}T_2, \beta^+ \geq 0.99)$ are given [13–16] by

$$T_0 = (D_0 + I_0 - \phi_0^+)/(41.3 \pm 2.2)R \quad (9)$$

$$T_1 = (D_1 + I_1 - \phi_1^+)/(28.4 \pm 1.3)R \quad (10)$$

$$T_2 = (\phi_2 - I_2)/(5.47 \pm 0.30)R \quad (11)$$

Here, D_0, I_0 and ϕ_0^+, for example, are the dissociation energy of MX, ionization energy of M and the work function of the ionizing surface, respectively, at T_0. The empirical constants (41.3, 28.4 and 5.47) are applicable to a great many sample/surface systems within experimental errors of about ±5%, independently of P, N and the species of both sample and surface employed. Generally, OTR becomes wider as I and ϕ become smaller and larger, respectively [6]. In contrast to T_1 and T_2, T_0 has no special theoretical meaning. Experimentally, however, T_0 is very important and interesting [13].

The effect of the substrate metal upon β^+ is examined with the common sample (KCL) at $N \approx 3 \times 10^{13}$ molecules cm^{-2} s^{-1} and $P \approx 2 \times 10^{-5}$ Pa, as shown in Fig. 4. The patterns of both β^+ and ϕ^+ are considerably different among the four systems especially in the range below ca. 1500 K. This difference is also observed with MCl/surface systems (see Fig. 5). In the high temperature range above T_3, however, ϕ^+ of each surface is virtually constant with little dependence upon any of T, N and sample species (see Fig. 5 and Table 1).

In order to clarify the effect of RG upon T_3, the temperature dependence of β^+ and hence of ϕ^+ is

Table 1
Effective work functions (ϕ^+ and ϕ^e) determined with polycrystalline metal surfaces under various experimental conditions. Curve numbers are common in Figs. 3–8

Curve	Surface	P	Sample	Flux	T_0	T_1	T_2	T_3	ϕ^+ or ϕ^e/kJ mol^{-1}						
		(*)		(**)	(K)	(K)	(K)	(K)	1000 K	1200 K	1400 K	1600 K	1800 K	2000 K	2200 K
—	Nb	2	RbCl	0.53	820	1420	1650	~1900	578	511	511	—	474	465	—
—	Nb	2	RbCl	0.80	830	1420	1650	~1900	578	528	500	—	474	464	—
—	Nb	2	RbCl	1.50	930	1460	1650	~1900	546	530	490	—	483	468	467
(9)	Nb	2	RbCl	2.74	940	1490	1610	~1900	546	545	498	~511	480	468	467
(15)	Nb	2	RbBr	1.62	850	1300	1550	~1900	519	492	—	490	476	463	—
—	Nb	2	RbBr	3.56	870	1330	1590	~1900	522	494	—	504	477	465	—
—	Nb	2	RbBr	7.28	890	1360	1570	~1900	527	498	—	499	476	464	—
—	Nb	2	RbI	1.41	980	1160	1280	~1900	425	—	457	457	458	457	453
—	Nb	2	RbI	2.64	990	1160	1280	~1900	424	—	461	461	462	461	461
(15′)	Nb	2	no	0	—	—	—	~1900	—	—	—	414	396	387	—
—	Mo	2	KCl	0.93	960	1220	1680	~2000	528	550	493	508	501	494	492
—	Mo	2	KCl	2.01	980	1255	1680	~2000	—	559	511	—	499	490	490
(5)	Mo	2	KCl	2.99	990	1490	1700	~2000	529	556	506	—	504	494	493
—	Mo	2	KBr	0.91	1000	1180	1645	~2000	—	—	522	—	493	473	473
(16)	Mo	2	KBr	2.92	1045	1210	1680	~2000	—	—	—	—	492	472	472
—	Mo	2	KBr	6.07	1080	1230	1700	~2000	—	522	—	—	500	473	474
—	Mo	2	KBr	9.70	1100	1250	1650	~2000	—	533	—	—	500	474	473
(16′)	Mo	2	no	0	—	—	—	~2000	—	—	—	473	445	423	423
—	Mo	20	no	0	—	—	—	~2000	—	—	519	487	465	439	428
(6)	Ta	2	KCl	2.96	950	—	—	~1800	528	505	501	491	491	492	492
—	Ta	2	RbCl	1.32	870	1470	1660	~1800	549	504	508	—	499	495	494
(10)	Ta	2	RbCl	3.68	915	1490	1730	~1800	549	506	506	—	512	500	498
—	Ta	2	RbBr	1.18	960	1350	1600	~1800	470	484	—	506	494	491	492
(17)	Ta	2	RbBr	2.24	965	1360	1610	~1800	472	485	—	—	494	494	494
—	Ta	2	RbBr	3.91	975	1370	1595	~1800	—	487	—	506	495	495	496
—	Ta	2	RbBr	7.98	990	1415	1630	~1800	472	485	504	—	495	495	495
—	Ta	2	CsF	1.09	980	1060	—	—	593	—	—	—	—	—	—
—	Ta	2	CsF	3.18	990	1090	—	—	578	—	—	—	—	—	—
—	Ta	2	CsF	6.94	1020	1120	—	—	—	—	—	—	—	—	—
—	Ta	2	CsCl	0.59	835	1420	—	—	543	494	497	—	—	—	—
—	Ta	2	CsCl	1.23	890	1460	—	—	543	497	493	—	—	—	—
—	Ta	2	CsCl	3.51	915	1480	—	—	543	504	499	—	—	—	—
—	Ta	2	CsCl	7.01	930	1500	—	—	543	520	497	—	—	—	—
(17′)	Ta	2	no	0	—	—	—	~1800	—	—	—	418	412	412	411
—	W	2	LiF	3.81	1060	—	—	~1950	—	738	665	601	550	500	496
—	W	2	LiF	6.55	1060	—	—	~1950	—	677	652	607	556	514	505
—	W	2	LiCl	1.30	1030	—	—	~1950	—	646	608	551	518	499	499
—	W	2	LiCl	2.76	1060	—	—	~1950	—	648	622	559	522	499	499
—	W	2	LiCl	5.77	1090	—	—	~1950	—	651	636	570	526	501	501
—	W	2	LiCl	11.1	1095	—	—	~1950	—	655	643	579	531	505	505
—	W	2	LiBr	1.39	1070	1220	1375	~1950	—	660	601	554	528	503	503
—	W	2	LiBr	4.01	1090	1245	1370	~1950	—	651	606	555	527	504	504
—	W	2	LiBr	5.52	1105	1265	1370	~1950	—	647	615	555	527	504	504
—	W	2	LiBr	11.0	1140	1275	1360	~1950	—	631	621	555	525	504	504
—	W	20	LiBr	3.72	1040	1330	1410	~2100	—	653	636	577	549	511	505
—	W	2	LiI	0.55	1135	1140	1370	~1950	—	—	584	553	523	509	509
—	W	2	LiI	1.61	1195	1205	1365	~1950	—	554	580	552	526	508	508

Table 1
(Continued)

Curve	Surface	P	Sample	Flux	T_0	T_1	T_2	T_3	ϕ^+ or ϕ^e/kJ mol^{-1}						
		(*)		(**)	(K)	(K)	(K)	(K)	1000 K	1200 K	1400 K	1600 K	1800 K	2000 K	2200 K
—	W	2	LiI	4.34	1210	1225	1375	~1950	—	—	593	554	532	506	507
(1)	W	2	NaCl	1.60	880	1250	1400	~1950	617	628	594	551	525	503	504
(2)	W	2	NaCl	3.10	920	1280	1410	~1950	603	624	—	555	528	503	503
—	W	2	NaCl	4.52	925	1290	1400	~1950	600	619	~588	553	524	503	503
(3)	W	2	NaCl	7.35	965	1325	1415	~1950	600	621	—	554	522	501	503
—	W	2	NaCl	14.0	980	1320	1400	~1950	603	621	606	552	513	499	501
(4)	W	2	NaCl	22.0	1000	1345	1420	~1950	591	617	—	560	524	504	506
—	W	2	NaBr	0.61	930	1020	1400	~1960	578	>578	~569	550	524	501	501
(18)	W	2	NaBr	1.87	985	1060	1400	~1960	564	>578	~569	551	526	502	502
—	W	2	NaBr	4.02	1010	1090	1400	~1970	555	>578	~569	553	525	503	504
—	W	2	NaI	0.54	1000	1005	1350	~1970	—	—	569	548	521	507	507
—	W	2	NaI	1.51	1030	1035	1320	~1970	—	—	567	548	521	505	506
—	W	2	NaI	4.41	1050	1070	1390	~1970	—	—	569	549	522	501	502
—	W	2	NaI	13.6	1090	1110	1380	~1970	—	—	576	549	528	503	503
—	W	2	KF	3.72	980	990	1870	~1970	—	—	—	—	—	497	494
—	W	2	KF	7.95	995	1005	1850	~1970	—	—	—	—	—	493	492
—	W	2	KCl	0.43	855	1145	1750	~1950	565	—	—	—	518	488	492
—	W	2	KCl	1.23	870	1205	1760	~1950	561	590	—	—	522	489	493
(7)	W	2	KCl	3.78	900	1240	1760	~1950	559	589	—	—	521	490	492
—	W	2	KCl	13.4	920	1260	1720	~1950	551	586	—	—	522	490	491
—	W	2	KCl	22.5	955	1290	1740	~1950	551	586	—	—	521	491	492
—	W	2	KBr	1.81	890	960	1950	~1950	—	—	—	—	508	487	488
—	W	2	RbCl	2.50	840	1050	1955	~1970	587	—	—	—	—	505	494
—	W	2	RbCl	5.50	850	1070	1970	~1970	585	—	—	—	—	518	497
—	W	2	RbCl	10.0	870	1100	1950	~1970	578	—	—	—	—	507	494
—	W	2	TlCl	0.52	850	1255	1350	—	—	657	616	—	—	—	—
—	W	2	TlCl	0.95	910	1275	1340	—	—	657	611	—	—	—	—
—	W	2	TlCl	2.49	950	1290	1350	—	—	659	614	—	—	—	—
—	W	2	TlCl	6.02	980	1300	1340	—	—	658	618	—	—	—	—
—	W	2	TlCl	9.13	1005	1315	1340	—	—	654	620	—	—	—	—
—	W	20	TlCl	6.50	980	1305	1390	—	—	656	680	—	—	—	—
—	W	200	TlCl	6.39	960	1405	1430	—	—	651	—	593	—	—	—
—	W	2	TlI	0.47	1030	1090	1165	—	—	646	599	—	—	—	—
—	W	2	TlI	1.73	1050	1105	1175	—	—	649	591	—	—	—	—
—	W	2	TlI	3.63	1065	1120	1180	—	—	657	596	—	—	—	—
—	W	10	TlI	1.45	1035	1130	1170	—	—	652	616	577	—	—	—
—	W	2	InI	1.68	1070	1110	1280	—	—	—	571	—	—	—	—
—	W	2	InI	3.55	1080	1130	1270	—	—	—	575	—	—	—	—
(18′)	W	2	no	0	—	—	—	~2000	—	—	—	478	449	432	431
—	W	2	no	0	—	—	—	~2100	—	—	—	492	465	439	428
—	Re	2	LiCl	0.41	1010	1360	1430	~1750	—	673	—	551	530	531	—
—	Re	2	LiCl	1.79	1025	1390	1450	~1750	—	672	—	557	534	535	—
—	Re	2	LiCl	4.09	1065	1400	1460	~1750	—	661	—	584	535	534	—
—	Re	2	LiCl	12.30	1075	1470	1510	~1750	—	647	—	571	536	533	—
(19)	Re	2	LiBr	1.87	1090	1240	1390	~1750	—	646	631	542	528	528	—
—	Re	2	LiBr	5.90	1125	1300	1395	~1700	—	627	629	547	529	529	—
—	Re	2	LiBr	10.70	1135	1330	1425	~1700	—	607	—	551	529	529	—
—	Re	2	LiBr	17 30	1150	1350	1425	~1700	—	596	—	552	530	530	—
—	Re	2	LiI	0 46	1130	1180	1400	~1750	—	—	610	548	527	529	—
—	Re	2	LiI	8.10	1165	1270	1370	~1750	—	533	604	552	530	531	—

Table 1
(Continued)

Curve	Surface	P	Sample	Flux	T_0	T_1	T_2	T_3	ϕ^+ or ϕ^e/kJ mol^{-1}						
		(*)		(**)	(K)	(K)	(K)	(K)	1000 K	1200 K	1400 K	1600 K	1800 K	2000 K	2200 K
—	Re	20	LiI	10.30	1155	1270	1460	~1900	—	541	—	580	543	533	—
—	Re	2	NaCl	0.30	895	1050	1350	~1700	656	—	567	526	522	524	—
—	Re	2	NaCl	0.61	920	1120	1365	~1700	651	—	585	529	521	523	—
(11)	Re	2	NaCl	3.40	950	1160	1375	~1700	630	—	593	527	521	525	—
—	Re	2	NaCl	6.27	955	1180	1425	~1700	615	—	—	534	524	525	—
—	Re	2	NaI	0.56	945	1015	1260	~1750	542	—	557	534	520	523	—
—	Re	2	NaI	1.45	960	1050	1280	~1750	522	—	565	531	521	523	—
(12)	Re	2	NaI	4.85	995	1105	1300	~1750	504	—	571	538	522	525	—
(13)	Re	20	NaI	4.30	995	1040	1295	~1900	509	—	572	562	532	524	—
(14)	Re	200	NaI	4.37	995	1040	1300	~2050	—	—	571	564	550	526	—
—	Re	200	NaI	0.43	935	965	1270	~2050	521	—	568	564	550	525	—
(8)	Re	2	KCl	2.63	950	1260	—	—	579	576	—	—	—	—	—
—	Re	2	TlCl	1.21	960	1070	1100	—	676	632	577	—	—	—	—
—	Re	2	TlCl	2.61	965	1075	1110	—	677	642	582	—	—	—	—
—	Re	2	TlCl	5.88	970	1080	1110	—	678	656	587	—	—	—	—
—	Re	4	TlI	0.72	995	1025	1075	—	584	621	596	—	—	—	—
—	Re	4	TlI	1.27	1005	1030	1070	—	—	620	598	—	—	—	—
—	Re	4	TlI	3.48	1020	1055	1080	—	—	621	591	—	—	—	—
—	Re	10	TlI	1.61	1010	1040	1100	—	—	615	597	—	—	—	—
—	Re	2	InI	1.51	1030	1090	1160	—	—	619	—	—	—	—	—
(19′)	Re	2	no	0	—	—	—	~1750	—	—	—	495	478	477	—

The units in (*) and (**) are 10^{-5} Pa and 10^{13} molecules cm^{-2} s^{-1}, respectively.

examined with the NaI/Re system at different residual gas pressures, as shown in Fig. 6. As P is increased from 2×10^{-5} to 2×10^{-3} Pa by admission of air, curve (12) is shifted to curve (14), and hence, T_3, is increased from ca. 1750 to 2050 K. Namely, the lowest temperature (T_3) keeping the ionizing surface essentially clean becomes higher by ca. 300 K as P increases by 100 times. The data in Fig. 6 give additional evidence to support the above conclusion that the increase in ϕ^+ with decreasing temperature from T_3 is caused mainly by adsorption of RG.

Fig. 7 shows an example of a Richardson plot obtained with W at $P = 2 \times 10^{-5}$ Pa without sample beam incidence. From the slope of a linear part (above T_3) of curve (b), ϕ^e is determined to be 434 ± 6 kJ mol^{-1}, corresponding to the work function (ϕ_0^e) of the essentially clean surface of polycrystalline tungsten. The difference between lines (a) and (b) below T_3 is caused by adsorption of RG alone because a sample beam is not directed onto F during this experiment. Substitution of the data into Eq. (8) according to a simple method [3] yields the work function increase ($\Delta\phi^e$), as shown by curve (c). In this way, temperature dependence of ϕ^e is studied with other metals too, thereby yielding Fig. 8(B). Below ca. 1400 K, J^e is usually too weak to be measured correctly by our present detection system. The values of ϕ^+ determined with five metals are shown in Fig. 8(A), where MBr at $N \approx 2 \times 10^{13}$ molecules cm^{-2} s^{-1} is directed onto each metal surface at $P = 2 \times 10^{-5}$ Pa (see Table 1). The values of $\Delta\phi^*$ determined from these data are shown in Fig. 8(C), indicating that $\Delta\phi^*$ of each metal depends little upon T although both ϕ^+ and ϕ^e tend to increase with decreasing temperature from T_3. It should be noted that $\Delta\phi^*$ determined at temperatures much below T_3 is virtually equal to the contrast ($\Delta\phi_0^*$) observed with the clean surface at $T \geq T_3$.

4.2. Time variation

The experimental data and analytical results summarized in Section 4.1 lead to the conclusion that the increase in ϕ^+ and ϕ^e with decreasing temperature from T_3 is caused mainly by adsorption of RG rather than MX. In order to examine the conclusion by a

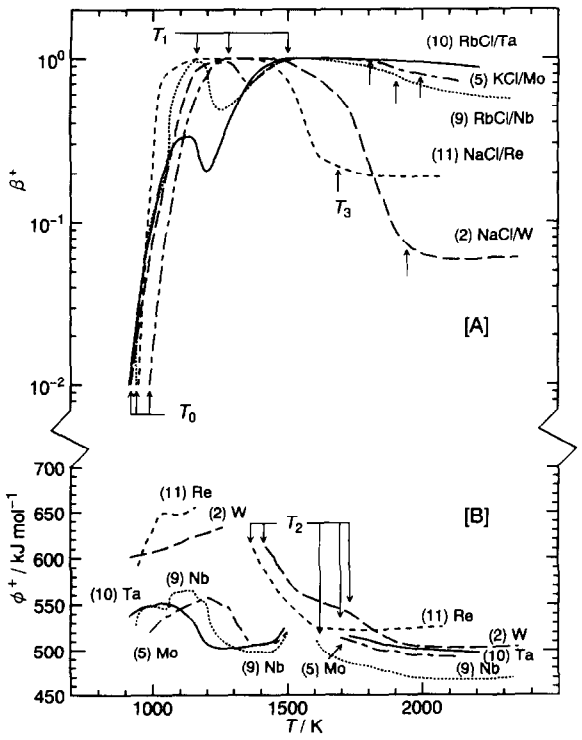

Fig. 5. Temperature dependence of (A) the ionization efficiency (β^+) of alkali chlorides (MCl) on five different metal surfaces and (B) the effective work function (ϕ^+) of the surface (see Table 1).

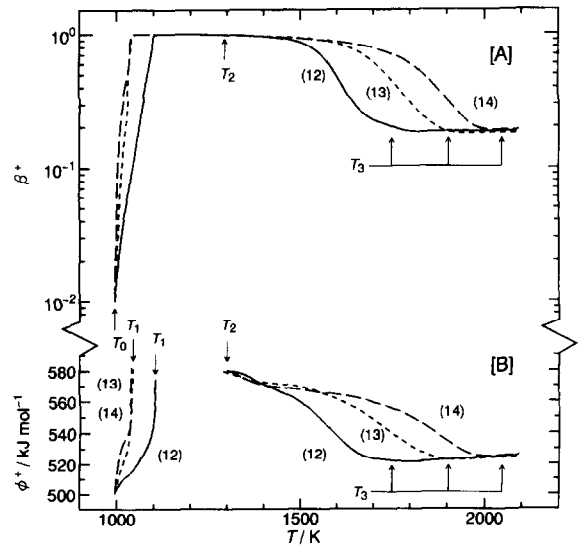

Fig. 6. Temperature dependence of (A) β^+ and (B) ϕ^+ observed with an NaI/Re system ($N \approx 4 \times 10^{13}$ molecules cm^{-2} s^{-1}) at different residual gas pressures of (12) 2×10^{-5}, (13) 2×10^{-4} and (14) 2×10^{-3} Pa (see Table 1).

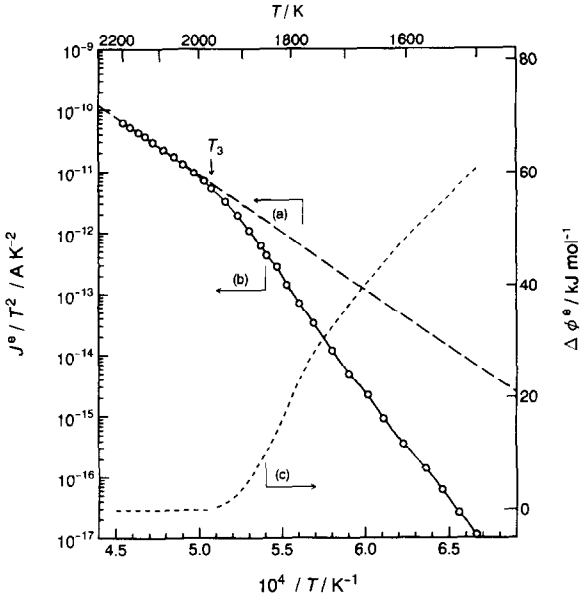

Fig. 7. Richardson plot obtained with W at the residual gas pressure of 2×10^{-5} Pa.

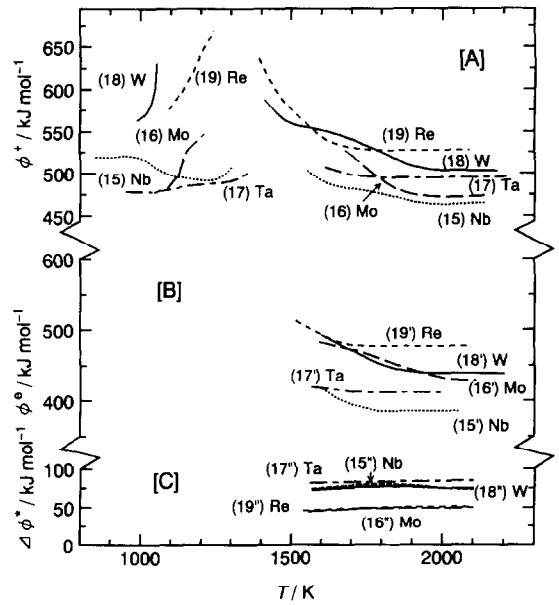

Fig. 8. Temperature dependence of (A) ϕ^+, (B) ϕ^e and (C) $\Delta\phi^*$ observed with five metal surfaces at 2×10^{-5} Pa. A beam of MBr at $n \approx 2 \times 10^{13}$ molecules cm^{-2} s^{-1} is employed for the determination of each ϕ^+ (see Table 1).

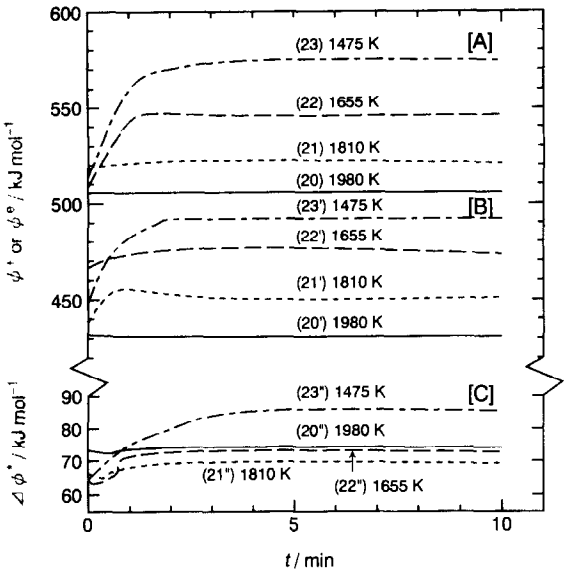

Fig. 9. Time variation of (A) the effective work function (ϕ^+) for the emission of Na^+ from NaCl/W system at $N = 1.04 \times 10^{14}$ molecules $cm^{-2}\ s^{-1}$, (B) the work function (ϕ^e) for thermal electron emission from W without sample beam incidence, and (C) the thermionic contrast ($\Delta\phi^*$) observed with W kept at each specified temperature in the residual gas pressure of 2×10^{-5} Pa.

different method, an additional study is made according to the procedures for time variation described in Section 2.

A typical example observed at ca. 2×10^{-5} Pa is summarized in Fig. 9, where curves (20)–(23) in [A] are obtained with an NaCl/W system at $N \approx 1.0 \times 10^{14}$ molecules $cm^{-2}\ s^{-1}$, while curves (20′)–(23′) are observed with W without sample beam incidence. Lines (20) and (20′) are independent of t, indicating that the surface of W heated to temperatures above T_3 (ca. 1950 K) is kept essentially clean without suffering from the incidence of both MX and RG. Below T_3, on the other hand, not only ϕ^+ but also ϕ^e increases rapidly up to respective saturation values within ca. 3 min, and the values tend to increase with a decrease in T. This tendency agrees well with the result exemplified in Fig. 3. In other words, any value of ϕ^+ or ϕ^e determined by temperature dependence below T_3 (see Fig. 8) corresponds to the saturation value at a given temperature. It is those saturation values that are listed in Table 1.

Curves (20″)–(22″) in Fig. 9(C) shows that $\Delta\phi^*$ observed much above T_2 (ca. 1400 K) is nearly constant at ca. 70 kJ mol^{-1}, virtually independent of both T and t. Compared with the value, $\Delta\phi^*$ shown by curve (23″) is larger by ca. 15 kJ mol^{-1}, thereby suggesting that the temporal increase in ϕ^+ from ca. 505 to 575 kJ mol^{-1} shown by curve (23) is caused partly (ca. 20%) by adsorption of NaCl at such a low temperature as 1475 K and also at a strong flux such ca. 1×10^{14} molecules $cm^{-2}\ s^{-1}$. This is consistent with the result that ϕ^+ at a temperature near $T_2 \approx 1400$ K tends to increase as N increases (see Fig. 3(C)).

The above results and conclusions are supported by our previous work, where work function changes are measured as a function of t under various conditions [10,17–24].

4.3. Introduction gas pressure dependence

As already described above, RG has the principal role in the work function increase observed even in a high vacuum (1×10^{-5} Pa). For a further study of this role by a different procedure, I^+ and I^e are measured separately as a function of the pressure (P_a) of introduced air, and the data obtained are analyzed to determine ϕ^+ and ϕ^e in a similar way as above. A typical example observed with an NaCl/Re system is shown in Fig. 10(A), where N is 4.67×10^{13} molecules $cm^{-2}\ s^{-1}$. It may be noted that curves (24) and (24′) observed at $P_a < 10^{-3}$ Pa correspond to ϕ_0^+ and ϕ_0^e, respectively. At any temperature, ϕ^+ as well as ϕ^e (see Fig. 10(B)) increases with an increase in P_a, and the work function increase at any pressure becomes larger with a decrease in T. However, $\Delta\phi^+$ itself is nearly constant at ca. 40 kJ mol^{-1} with little dependence upon T and P_a (see Fig. 10(C) and also Table 2), showing again that $\Delta\phi^*$ is virtually equal to $\Delta\phi_0^*$ under any experimental condition except a temperature range much below T_3.

Each of the perpendicular arrows in Fig. 10 indicates the highest pressure ($P_a^* \approx 1.3 \times 10^{-4}$ Pa at 1930 K, for example), only below which the rhenium surface heated to a specified temperature ($T^* = 1930$ K, for example) is kept virtually clean. In other words, T^* corresponds to the boundary temperature (T_3) explained in Section 4.1. Clearly, P_a^* increases as T_3 increases. The quantitative relation between the two for Re is illustrated in Fig. 11, which

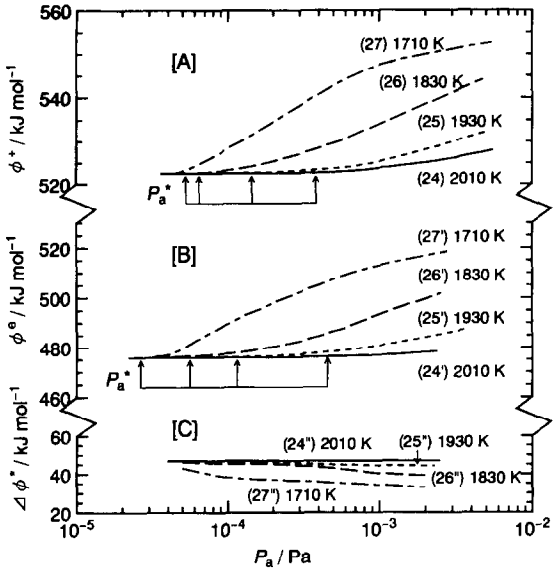

Fig. 10. Introduced air pressure (P_a) vs. (A) the work function (ϕ^+) determined with an NaCl/Re system ($N = 4.67\times 10^{13}$ molecules cm^{-2} s^{-1}), (B) the work function (ϕ^e) for electron emission from Re, and (C) the thermionic contrast ($\Delta\phi^*$) of Re kept at several temperatures (2101–1710 K). These data are listed in Table 2. With respect of P_a^*, see text.

cites the data on the NaCl/Re and NaI/Re systems exemplified in Figs. 10 and 6, respectively. In this way, Eqs. (12)–(14) are established with Re, W and Mo, respectively.

$$T_3 = (2685 \pm 67) + (209 \pm 18)\log P_a^* \quad (12)$$

$$T_3 = (2471 \pm 83) + (115 \pm 52)\log P_a^* \quad (13)$$

$$T_3 = (2468 \pm 43) + (100 \pm 42)\log P_a^* \quad (14)$$

where T_3 and P_a^* are expressed in K and Pa, respectively.

The results exemplified in Fig. 10 suggest that the work function increase with an increase in P_a is mainly due to the adsorption of O_2 included in the air introduced into the vacuum vessel. In order to examine this suggestion, both I^+ from an NaI/Re system at $N = 4.25 \times 10^{13}$ molecules cm^{-2} s^{-1} and J^e from Re without sample beam incidence are measured separately as a function of the oxygen pressure (P_0), and both ϕ^+ and ϕ^e are determined in the same way as above. Some of the results are summarized in Table 3 and also illustrated in Fig. 12, where $P_a/5$ as well as P_0 is taken as the abscissa because the former virtually corresponds to the partial pressure of O_2 in air, thereby making it ready to compare the two series of data on ϕ^+ or ϕ^e measured at the same pressure with respect to O_2. When T is as high as 2080 K, as shown by lines (28) and (29), ϕ^+ in air is the same with that in O_2 and both are little dependent upon the oxygen pressure, thus indicating that the surface is kept essen-

Table 2
Effective work functions (ϕ^+ and ϕ^e in kJ mol^{-1}) determined with Re as a function of introduced air pressure (P_a in Pa). A beam of NaCl at 4.67×10^{13} molecules cm^{-2} s^{-1} is employed for the determination of ϕ^+ (see Fig. 10)

Curve	T (K)	ϕ (kJ mol^{-1})	P_a/Pa						Mean (kJ mol^{-1})
			5×10^{-5}	1×10^{-4}	2×10^{-4}	5×10^{-4}	1×10^{-3}	2×10^{-3}	
(24)	2010	ϕ^+	522	523	523	523	524	525	523±2
(24')	2010	ϕ^e	476	476	476	476	477	478	476±2
(24")	2010	$\Delta\phi^*$	46	47	47	47	47	47	47±1
(25)	1930	ϕ^+	523	523	523	524	525	528	524±4
(25')	1930	ϕ^e	476	476	477	479	481	484	479±5
(25")	1930	$\Delta\phi^*$	47	47	46	45	44	44	46±2
(26)	1830	ϕ^+	523	523	525	530	534	538	—
(26')	1830	ϕ^e	476	478	480	487	494	500	—
(26")	1830	$\Delta\phi^*$	47	45	45	43	40	38	43±3
(27)	1710	ϕ^+	523	528	535	543	548	550	—
(27')	1710	ϕ^e	480	490	498	509	513	517	—
(27")	1710	$\Delta\phi^*$	43	38	37	34	35	33	37±6
Mean	2100–1710	$\Delta\phi^*$	46±3	44±6	44±7	42±8	42±6	41±7	—

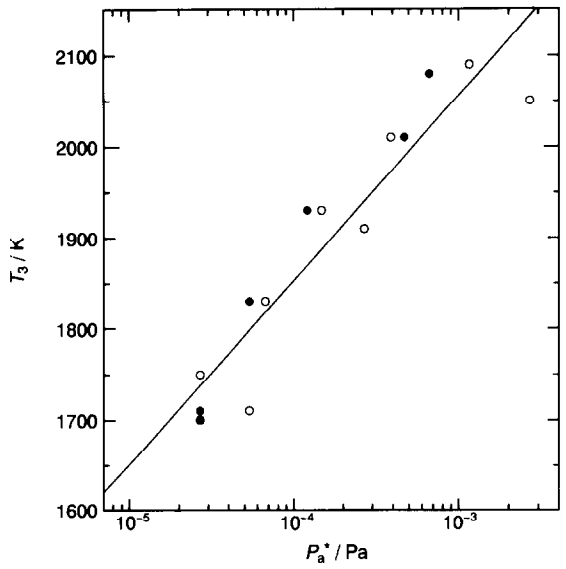

Fig. 11. Quantitative relation between the highest air pressure (P_a^*) and the lowest temperature (T_3) keeping the rhenium surface essentially clean (see Fig. 10). Open and solid circles are obtained from the data on the emissions of positive ions (Na^+ from NaCl or NaI at $N \approx 4 \times 10^{13}$ molecules $cm^{-2}\ s^{-1}$) and of electrons from Re, respectively.

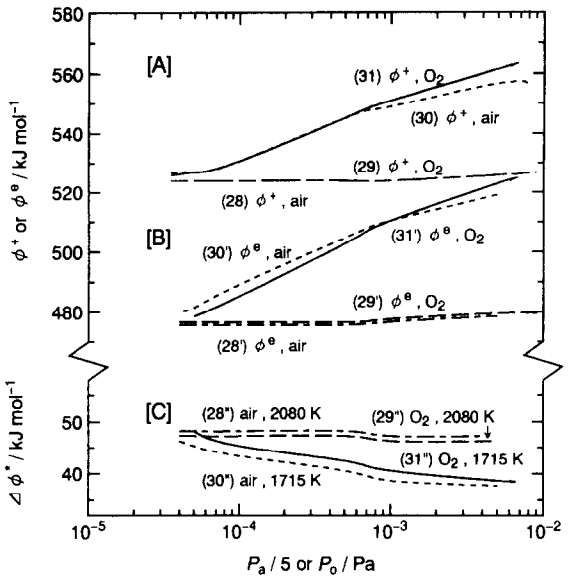

Fig. 12. Partial or total oxygen pressure ($P_a/5$ or P_0) vs. (A) the work function (ϕ^+) for the emission of Na^+ from an NaI/Re system (4.25×10^{13} molecules $cm^{-2}\ s^{-1}$), (B) the work function (ϕ^e) for thermal electron emission from Re, and (C) the thermionic contrast ($\Delta\phi^*$) observed with Re heated to (28)–(29) 2080 K or (30)–(31) 1715 K (see Table 3).

Table 3
Effect of partial or total oxygen gas pressure ($P_a/5$ or P_0 in Pa) upon the effective work functions (ϕ^+ and ϕ^e in kJ mol^{-1}) of polycrystalline rhenium (see Fig. 12). A beam of NaI at $N \approx 4 \times 10^{13}$ molecules $cm^{-2}\ s^{-1}$ is employed to determine ϕ^+

Curve	Gas	T (K)	ϕ (kJ mol^{-1})	$P_a/5$/Pa or P_0/Pa							Mean (kJ mol^{-1})
				5×10^{-5}	1×10^{-4}	2×10^{-4}	5×10^{-4}	1×10^{-3}	2×10^{-3}	5×10^{-3}	
(28)	air	2080	ϕ^+	524	524	524	524	524	524	525	524±0
(28′)	air	2080	ϕ^e	476	476	476	476	477	477	478	476±2
(28″)	air	2080	$\Delta\phi^*$	48	48	48	48	47	47	47	48±1
(29)	O_2	2080	ϕ^+	524	524	524	524	524	524	525	524±0
(29′)	O_2	2080	ϕ^e	477	477	477	477	478	478	479	478±1
(29″)	O_2	2080	$\Delta\phi^*$	47	47	47	47	46	46	46	47±1
(30)	air	1715	ϕ^+	526	529	534	542	548	552	556	—
(30′)	air	1715	ϕ^e	480	485	493	503	509	514	518	—
(30″)	air	1715	$\Delta\phi^*$	46	44	41	39	39	38	38	41±5
(31)	O_2	1715	ϕ^+	526	529	534	542	549	555	561	—
(31′)	O_2	1715	ϕ^e	477	483	489	499	508	514	522	—
(31″)	O_2	1715	$\Delta\phi^*$	49	46	45	43	41	41	39	43±6
Mean	air or O_2	2080–1715	$\Delta\phi^*$	48±2	46±2	45±4	44±4	43±4	43±5	43±5	—

tially clean so long as P_0 or $P_a/5$ is lower than 10^{-3} Pa. This is quite the same with regard to ϕ^e, as shown by lines (28′) and (29′). At a middle temperature such as 1715 K, on the other hand, all of the four work functions increase remarkably with an increase in oxygen pressure, as shown by curves (30)–(31) and (30′)–(31′). Again, however, ϕ^+ and ϕ^e in air are virtually equal to those in O_2, respectively, under the same oxygen pressure ($P_a/5 \approx P_0$). Consequently, the relation of T_3 to P_0^* for Re, for example, is expressed by

$$T_3 = (2831 \pm 67) + (209 \pm 18)\log P_0^* \qquad (15)$$

which is derived from Eq. (12).

The above results indicate that the work function increase is caused mainly by adsorption of O_2 and little by that of N_2 in air and also that the increase in ϕ^+ observed in the middle temperature range (see curve (12) in Fig. 6) is also caused mainly by adsorption of O_2 remaining as one of the residual gases. As shown in Fig. 12 and also listed in Table 3, the change in $\Delta\phi^*$ remains within ca. 10 kJ mol^{-1} even when P_a or P_0 increases by up to ca. 100 times.

Table 1 shows that ϕ^+ at temperature below T_2 has a strong dependence upon the species of MX and N owing to coadsorption of MX and RG. Above T_3, on the other hand, ϕ^+ is kept virtually constant at ϕ_0^+, without suffering from such an adsorption. As shown in Table 4, our data on ϕ_0^e are in good agreement with literature values [25], thereby indicating that our experiments are virtually free from systematic errors. With respect to ϕ_0^+, on the other hand, good agreement

Table 4
Data on the work functions (ϕ_0^+ and ϕ_0^e) determined with essentially clean surfaces of polycrystalline refractory metals heated in the residual gas pressure (P) of 10^{-4}–10^{-7} Pa. Here, X denotes hologen. No sample is employed during the determination of ϕ_0^e. The value of ϕ_0^e generally accepted with each surface is given in parenthesis

Surface	P/Pa	T/K	Sample	Ion	ϕ_0^+/kJ mol^{-1}	ϕ_0^e/kJ mol^{-1}	$\Delta\phi_0^*$/kJ mol^{-1}	Ref.
Nb	2×10^{-5}	1800–2200	RbX	Rb^+	463±10	388±5	75±10	Our work
Nb	—	—	—	—	—	(385)	—	[25]
Mo	2×10^{-5}	1900–2200	KX	K^+	480±6	424±4	56±6	Our work
Mo	1×10^{-5}	1900–2300	In	In^+	484±5	418±7	66±7	[26]
Mo	—	—	—	—	—	(415)	—	[25]
Ta	2×10^{-5}	1800–2200	KX, RbX, CsX	K^+, Rb^+, Cs^+	493±5	413±5	80±5	Our work
Ta	1×10^{-5}	1700–2200	In	In^+	471±5	418±3	53±5	[26]
Ta	1×10^{-7}	1900–2100	Na	Na^+	448±3	415±2	33±3	[27]
Ta	6×10^{-7}	2500–2800	Ba	Ba^+	408±3	404	~0	[28]
Ta	6×10^{-7}	2400–2800	Sr	Sr^+	402	404	~0	[28]
Ta	—	—	—	—	—	(398)	—	[25]
W	2×10^{-5}	1950–2200	LiX, NaX, KX, RbX	Li^+, Na^+, K^+, Rb^+	504±5	434±6	70±6	Our work
W	1×10^{-5}	2100–2600	In	In^+	496±3	442±3	54±3	[26]
W	6×10^{-7}	2500–2800	Ba	Ba^+	442	—	—	[28]
W	6×10^{-5}	2300–2700	In	In^+	487±5	442±5	45±5	[29]
W	1×10^{-4}	2000–2300	Cu, Ag	Cu^+, Ag^+	500–510	—	—	[30]
W	—	—	—	—	—	(435)	—	[25]
Re	2×10^{-5}	1800–2100	LiX, NaX	Li^+, Na^+	530±5	476±5	54±5	Our work
Re	1×10^{-5}	1750–2400	Ca	Ca^+	524±3	476±4	48±4	[26]
Re	6×10^{-7}	2000–2800	Ba, Sr	Ba^+, Sr^+	499	—	—	[28]
Re	6×10^{-5}	2300–2700	In	In^+	520±5	481±5	39±5	[29]
Re	1×10^{-6}	1600–2400	Li, LiX	Li^+	503±1	481±3	22±3	[31]
Re	—	—	—	—	—	(480)	—	[25]

is not always found between the present and published values. This is mainly because reliable data on ϕ_0^+ have not yet fully been published to date, in contrast to those on ϕ_0^e. In addition, the dependence of ϕ^+ upon the experimental conditions such as T, P and N has not been reported by any other group of workers. This is the reason why we summarize our data in Tables 1–3. It should be emphasized that such a dependence of ϕ^+ can hardly be clarified without using Eqs. (4)–(7), the validity of which has already been confirmed [2].

5. Conclusions

The above experimental data and analytical results exemplified in Figs. 3–12 and Tables 1–4 lead to the conclusions as follows:

1. The effective work function (ϕ^+) of polycrystal metals strongly depends upon surface temperature (T) and upon residual and/or introduced gas pressure (P) even at high temperatures (usually above ca. 1400 K) mainly because of gas adsorption, and also ϕ^+ depends upon the sample species and flux at low temperatures (usually below ca. 1300 K) owing to coadsorption of the gases and sample molecules. Consequently, ϕ^+ is increased by up to ca. 150 kJ mol^{-1} according to the conditions of T, P, N employed and the species of both sample and substrate metal.
2. In the temperature range ($T > T_3$) high enough to keep the surface essentially clean, the work function (ϕ_0^+) is kept nearly constant and depends only upon the species of metal, ranging from 463 kJ mol^{-1} (Nb) up to 530 kJ mol^{-1} (Re). When ϕ_0^+ of some metal is employed for evaluating β^+ from Eqs. (4)–(7), therefore, T_3 should be checked under the experimental condition to be employed because T_3 itself depends upon P.
3. The temperatures of T_3 found with five metals are virtually common to ϕ^+ and ϕ^e of each metal. The values of ϕ_0^e determined above T_3 range from 388 kJ mol^{-1} (Nb) to 476 kJ mol^{-1} (Re), in good agreement with literature values generally accepted to date.
4. Dependence of ϕ^e upon the experimental conditions mentioned above is nearly the same as that of ϕ^+, thereby yielding that the thermionic contrast ($\Delta\phi^* \equiv \phi^+ - \phi^e$) observed under any condition except a low temperature range much below T_3 is equal to $\Delta\phi_0^*$ found only above T_3 and also that $\Delta\phi^*$ and $\Delta\phi_0^*$ range from 54 kJ mol^{-1} (Re) up to 80 kJ mol^{-1} (Ta). According to these data, therefore, ϕ^+ or ϕ_0^+ may be evaluated readily from either those data on ϕ^e determined under a specified condition or literature values of ϕ_0^e.

Further work, however, is necessary to clarify the fine mechanism of the work function changes due to adsorption of residual gases and/or sample molecules.

Acknowledgements

This work was partly supported by a Research Grant (No. 06650041) from the Ministry of Education, Science and Culture and also by that (No. 951118) from The Murata Science Foundation.

References

[1] H. Kawano and F.M. Page, Int. J. Mass Spectrom. Ion Phys., 50 (1983) 1.
[2] H. Kawano and T. Kenpō, J. Chem. Phys., 81 (1984) 6310.
[3] H. Kawano, S. Itasaka, S. Ohnishi and Y. Hidaka, Int. J. Mass Spectrom. Ion Proc., 70 (1986) 195.
[4] D.R. Stull and H. Prophet, JANAF Thermochemical Tables, 2nd edn., NBS, Washington, 1971.
[5] I. Barin, Thermochemical Data of Pure Substances, VCH, Weinheim, 1989.
[6] H. Kawano, S. Matsui and N. Serizawa, Rev. Sci. Instrum., 67 (1996) 1193.
[7] H. Kawano, T. Kenpō and Y. Hidaka, Bull. Chem. Soc. Jpn., 57 (1984) 581.
[8] H. Kawano and T. Kenpō, Bull. Chem. Soc. Jpn., 57 (1984) 1415.
[9] H. Kawano and T. Kenpō, Bull. Chem. Soc. Jpn., 57 (1984) 3399.
[10] H. Kawano and T. Kenpō, Int. J. Mass Spectrom. Ion Proc., 66 (1985) 93.
[11] H. Kawano, Y. Kutsuna, K. Ohgami and K. Funato, Appl. Surf. Sci., 70/71 (1993) 158.
[12] H. Kawano, K. Ohgami, K. Funato and J. Nakamura, Vacuum, 46 (1995) 1139.
[13] H. Kawano, S. Kaneda, H. Karigō, Y. Kutsuna and Y. Hidaka, Int. J. Mass Spectrum. Ion Proc., 94 (1989) 179.
[14] H. Kawano, K. Ohgami, S. Matsui and Y. Kitayama, Appl. Surf. Sci., 100/101 (1996) 193.
[15] H. Kawano, S. Matsui and Y. Zhu, Appl. Surf. Sci., 108 (1997) 113.

[16] H. Kawano, K. Ohgami, S. Matsui and Y. Zhu, to be published.
[17] H. Kawano, T. Kenpō and Y. Hidaka, Int. J. Mass Spectrum. Ion Proc., 62 (1984) 137.
[18] H. Kawano and T. Kenpō, J. Chem. Phys., 81 (1984) 1248.
[19] H. Kawano and T. Kenpō, Int. J. Mass Spectrum. Ion Proc., 65 (1985) 299.
[20] H. Kawano, T. Kenpō and Y. Hidaka, Int. J. Mass Spectrom. Ion Proc., 67 (1985) 137.
[21] H. Kawano, S. Itasaka and S. Ohnishi, Int. J. Mass Spectrum. Ion Proc., 73 (1986) 145.
[22] H. Kawano, Y. Kutsuna, K. Ohgami and K. Funato, Appl. Surf. Sci., 70/71 (1993) 158.
[23] H. Kawano, K. Ohgami, K. Funato and J. Nakamura, Vacuum, 46 (1995) 1145.
[24] H. Kawano, K. Ohgami, K. Funato and J. Nakamura, Appl. Surf. Sci., 70/71 (1993) 142.
[25] V.S. Fomenko, Handbook of Thermionic Properties, Plenum Press, New York, 1996.
[26] É.Ya. Zandberg and A.Ya. Tontegode, Sov. Phys. Tech. Phys., 10 (1966) 1162.
[27] É.P. Sytaya and N.G. Shuppe, Sci. Trans. Tashkent Univ., 221 (1963) 103 [Chem. Abstr., 60 (1964) 15248e] [English translation available from Natl. Tech. Inf. Service, Springfield, VA 22151, U.S.A.; Order No. AD-668504].
[28] J.R. Werning, U.S. Atomic Energy Commission, UCRL-8455 (1958) [Chem. Abstr., 53 (1959) 13785i].
[29] N.D. Konovalov, V.A. Kuznetsov and B.M. Tsarev, Sov. Phys. Tech. Phys., 14 (1969) 834.
[30] I.N. Bakulina and N.I. Ionov, Sov. Phys. Dokl., 9 (1964) 217.
[31] E.N. Sloth, M.H. Studier and P.G. Wahlbeck, J. Phys. Chem., 78 (1974) 820.